Iterative and Power Series Solutions for the Large Deflection of an Annular Membrane

ALLAN B. PIFKO* AND MARTIN A. GOLDBERG†
Grumman Aircraft Engineering Corporation, Bethpage, N. Y.

Nomenclature

a, b, λ = inner, outer, and radius ratio (a/b) of annulus, respectively
E, ν = modulus of elasticity and Poisson's ratio, respectively
h = thickness
q = normal load intensity
r, ρ = physical and dimensionless (r/b) coordinates, respectively
S_r, S_θ = dimensionless stress resultants, $(h^2/q^2b^2E)^{1/3}(\sigma_r, \sigma_\theta)$
U = dimensionless radial displacement, $(hE/qb)^{2/3}(u/b)$
W = dimensionless deflection, $(hE/qb)^{1/3}(w/b)$

Introduction

IN previous papers, [1, 2] an iterative technique was employed to obtain approximate closed form solutions for the large deflection of uniformly loaded circular plates and membranes. A comparison of some of these solutions with more exact results[3–5] indicated that the iterative procedure is suitable for engineering analysis. However, since the solutions compared were characterized by a relatively uniform in-plane stress field, the question arose regarding the accuracy and convergence of the iterative technique when the variation of the membrane stresses is more pronounced. This led to the investigation of the large deflection of a uniformly loaded annular membrane fixed at the outer boundary and free of tractions and support at the inner boundary.

Earlier results[2] indicate that the membrane stresses associated with this problem vary significantly near the free boundary. These results, which constitute a first approximate solution, are used herein to obtain a second approximate solution by the iterative technique. In addition, a power-series solution to the problem is presented. The accuracy of the approximate solution[6] is then demonstrated by comparison with the power-series solution for a range of inner to outer radius ratios, λ.

Governing Equations

The large deflection of an initially flat elastic membrane, described by the Föppl-Hencky theory,[2] is characterized by two coupled nonlinear partial differential equations. For the problem under consideration, the dimensionless form of these equations, in rotationally symmetric polar coordinates, is

$$\rho \frac{d}{d\rho}\left[\frac{1}{\rho}\frac{d}{d\rho}(\rho^2 S_r)\right] = \frac{1}{2}\left(\frac{dW}{d\rho}\right)^2 \tag{1}$$

$$\rho S_r \frac{dW}{d\rho} = \frac{1}{2}(\lambda^2 - \rho^2) \tag{2}$$

where Eq. (2) is the first integral of the vertical equilibrium equation, subject to the condition of a vanishing vertical force at the inner edge, $\rho = \lambda$. The associated stress-strain and strain-displacement relations are taken in the usual form.

Received December 31, 1963; revision received March 19, 1964.

* Research Engineer, Research Department.
† Formerly Head of Applied Mechanics, Research Department; now Specialist Engineer, Structural Development Section, Engineering Division, Republic Aviation Corporation, Farmingdale, N.Y.

For subsequent use in the iterative technique, we require the dilatation equation

$$\frac{1}{\rho}\frac{d}{d\rho}(\rho U) + \frac{1}{2}\left(\frac{dW}{d\rho}\right)^2 = \frac{(1-\nu)}{\rho}\left[\frac{d}{d\rho}(\rho^2 S_r)\right] \tag{3}$$

which relates the sum of the principal strains to the mean stress.

The formulation of the problem is completed by specifying the remaining boundary conditions. They are, for an annular membrane fixed at the outer edge, and free of tractions and support at the inner edge,

$$W = U = 0 \quad \text{at} \quad \rho = 1 \tag{4a}$$

$$S_r = 0 \quad \text{at} \quad \rho = \lambda \tag{4b}$$

Iterative Procedure

The first step of the procedure is to neglect the right-hand side of Eq. (1), and solve

$$\rho\left(\frac{d}{d\rho}\right)\left[\left(\frac{1}{\rho}\right)\left(\frac{d}{d\rho}\right)(\rho^2 S_r)\right] = 0 \tag{5}$$

for S_r. However, since Eq. (5) is uncoupled from the transverse equilibrium equation (2), satisfaction of all the in-plane boundary conditions associated with Eq. (5) cannot explicitly relate the normal load to the membrane stresses. Therefore, only one of the in-plane boundary conditions is satisfied, and the remaining unknown constant regulates the magnitude of the stresses. Furthermore, this constant serves to relate the normal load on the membrane to the in-plane stress field. Thus, the first approximation for the stresses S_r^I comprises the functional form given by the solution to Eq. (5), multiplied by an undetermined "characteristic unknown" constant, α_1.

We then put S_r^I in Eq. (2) and solve for the first approximation to the deflection W_I. The constant α_1 is evaluated by establishing a displacement field U, which is compatible with the stress field S_r^I and the normal deflection W_I. To this end we put S_r^I and W_I into Eq. (3) and solve for U. Satisfying the required boundary conditions then determines the characteristic unknown, α_1. A refined first approximation for the radial stress is now found by putting W_I in Eq. (1) and solving for a new stress. This stress, denoted by S_r^{IR}, is explicitly associated with the deflection, whereas S_r^I is only implicitly related to the deflection through α_1. This completes the first approximate set of solutions, namely, W_I, α_I, and S_r^{IR}.

Further iterations can be found in an analogous manner. In continuing the process, we take the next iteration S_r^{II} to be composed of the functional form as given by S_r^{IR}, multiplied by a new characteristic unknown, α_2. Following the same procedure just outlined, we arrive at the second set of approximate solutions, namely, W_{II}, α_2, and S_r^{IIR}. Proceeding formally, we can obtain an nth set of approximate solutions.

Approximate Solutions

Since the first iteration to this problem was presented previously,[2] it suffices only to record the numerical results obtained (Figs. 1–3).

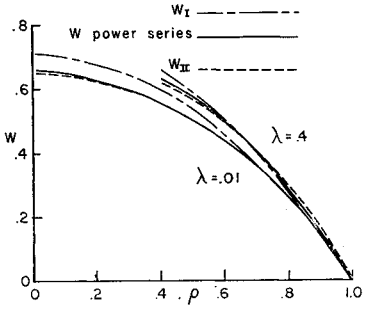

Fig. 1 Comparison of W_I and W_{II} with W, the power series solution, for λ = 0.01, 0.4.

Table 1 Coefficients a_1, with $\nu = 0.3$, for various radius ratios

λ:	0	0.01	0.1	0.2	0.3	0.4
a_1:	1.7245	1.724	1.713	1.678	1.625	1.553

In accordance with the iterative procedure, the second approximation for the radial stress is $S_r^{II} = \alpha_2 S_r^{IR}$, where S_r^{IR} is given in Ref. 2 and α_2 is a characteristic unknown. Then, after substituting S_r^{II} into Eq. (2), integrating, and making use of Eq. (4), we obtain the second approximation for the deflection

$$W_{II} = \frac{\alpha_1^2}{\alpha_2}\left(\frac{2}{1-\nu}\right)^{2/3} \times \ln\left[\frac{3-\nu-(1-\nu)(\lambda^2+\rho^2)-(1+\nu)\lambda^2\rho^2}{2(1-\lambda^2)}\right] \quad (6)$$

where

$$\alpha_1^3 = \frac{(1-\nu)(1-\lambda^4)}{1-\nu+(1+\nu)\lambda^2}$$

To find α_2, we put S_r^{II} and W_{II} into Eq. (3) and integrate to obtain the radial displacement. Satisfaction of the boundary conditions leads to the expression for the characteristic unknown,

$$\alpha_2^3 = \frac{8\alpha_1^6}{(1-\nu)^2(1-\lambda^4)} \times \left\{\frac{3-\nu-(1-\nu)\lambda^2}{2(M-\lambda^2)} - \ln\left[\frac{3-\nu+(1+\nu)\lambda^2}{2}\right]\right\} \quad (7)$$

with

$$M = \frac{3-\nu-(1-\nu)\lambda^2}{1-\nu+(1+\nu)\lambda^2}$$

To find the refined second approximation to the stress, we substitute W_{II} into Eq. (1) and solve the resulting equation, subject to the boundary conditions, and obtain

$$S_r^{IIR} = \left(\frac{1}{2}\right)\frac{\alpha_1^4}{\alpha_2^2}\left(\frac{2}{1-\nu}\right)^{4/3}\left(\frac{1}{1-\nu+(1+\nu)\lambda^2}\right) \times \left\{\frac{2}{M-1}\left(1-\frac{\lambda^2}{\rho^2}\right) - (1+\nu)\ln\left(\frac{M-\lambda^2}{M-1}\right) + \frac{1}{\rho^2}\left[(1-\nu)\ln\frac{M-\rho^2}{M-\lambda^2} + (1+\nu)\lambda^2\ln\frac{M-\rho^2}{M-1}\right]\right\} \quad (8a)$$

and, from the in-plane equilibrium equation,

$$S_\theta^{IIR} = (d/d\rho)(\rho S_r^{IIR}) \quad (8b)$$

Equations (6–8) constitute the second set of approximate solutions to Föppl's equations, (1) and (2).

Exact Solution

The power-series analysis will be facilitated by introducing the transformations $f = \rho^2 S_r$ and $\xi = \rho^2$ into Eqs. (1) and (2). After solving for $dW/d\xi$ from Eq. (2) and substituting the result into Eq. (1), we arrive at the controlling nonlinear differential equation

$$f^2(d^2f/d\xi^2) = -\tfrac{1}{32}(\lambda^2-\xi)^2 \quad (9)$$

The transformed boundary conditions associated with Eq. (9) are,

$$2\frac{df}{d\xi} - (1+\nu)f = 0 \quad \text{at} \quad \xi = 1 \quad (10a)$$

$$f = 0 \quad \text{at} \quad \xi = \lambda^2 \quad (10b)$$

We now solve Eq. (9) by assuming that $f(\xi)$ can be written as

$$f(\xi) = \frac{1}{4}\sum_{n=1}^{\infty} a_n(\xi-\lambda^2)^n \quad (11)$$

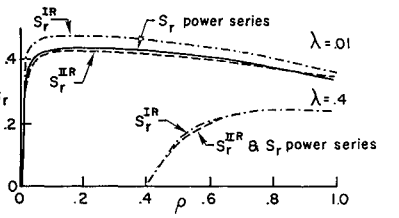

Fig. 2 Comparison of S_r^{IR} and S_r^{IIR} with S_r, the power series solution, for $\lambda = 0.01, 0.4$.

The coefficients a_n are evaluated in the usual manner[6] and are, in terms of a_1,

$$a_2 = -(1/a_1^2) \quad (12a)$$

$$a_n = -\frac{1}{n(n-1)a_1^2}\sum_{m=3}^{n}(n-m+2) \times (n-m+1)a_{n-m+2}b_m \qquad n > 2 \quad (12b)$$

with

$$b_m = \sum_{m=0}^{n} a_m a_{n-m} \quad (12c)$$

To determine a_1, we put Eq. (11) into Eq. (10a), and after making use of (12), arrive at an algebraic equation[6] involving a_1 and λ only. The solution of this equation for selected values of λ yields values of a_1 as shown in Table 1.

Thus, the function $f(\xi)$ is completely determined and is

$$f(\xi) = (a_1^4\Phi/4)\left[1 - \Phi - \tfrac{2}{3}\Phi^2 - \tfrac{13}{18}\Phi^3 - \tfrac{17}{18}\Phi^4 - \tfrac{37}{27}\Phi^5 - \tfrac{1205}{567}\Phi^6 \ldots\right] \quad (13a)$$

with

$$\Phi = (\xi - \lambda^2)/a_1^3 \quad (13b)$$

The radial stress is found from the definition of $f(\xi)$, and the circumferential stress follows directly from the in-plane equilibrium equation (8b). To find W, we put Eq. (13a) into Eq. (2), invert the series, and integrate termwise to obtain

$$W = \frac{1}{a_1}\left\{1 - \xi + \frac{1}{2a_1^3}[(1-\lambda^2)^2 - (\rho^2-\lambda^2)^2] + \frac{5}{9a_1^6}[(1-\lambda^2)^3 - (\rho^2-\lambda^2)^3] + \frac{55}{72a_1^9}[(1-\lambda^2)^4 - (\rho^2-\lambda^2)^4] + \frac{7}{6a_1^{12}}[(1-\lambda^2)^5 - (\rho^2-\lambda^2)^5] + \ldots\right\} \quad (14)$$

Equations (13a, 13b, and 14) constitute the exact solution to Föppl's equations, Eqs. (1) and (2).

Numerical Results

Numerical results obtained by the iteration procedure and the power-series solution are shown in Figs. 1–3 for selected

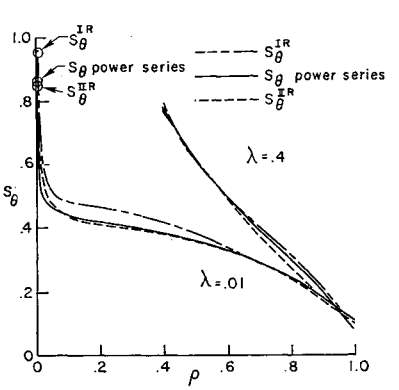

Fig. 3 Comparison of S_θ^{IR} and S_θ^{IIR} with S_θ, the power series solution, for $\lambda = 0.01, 0.4$.

values of the radius ratio[6] λ and for Poisson's ratio equal to 0.3.

Comparison of the iterative solutions with the more accurate power-series solution demonstrates the rapid convergence of the approximate solutions. Indeed, the agreement between the stresses and deflection predicted by the second approximation is within 1% of the results given by the series solution. Thus, the second iteration is in essence an approximate closed form representation of the exact series solution.

References

[1] Goldberg, M. A., "A modified large deflection theory of plates," *Proceedings of the Fourth U. S. National Congress of Applied Mechanics* (American Society of Mechanical Engineers, New York, 1962), pp. 611–618.

[2] Goldberg, M. A. and Pifko, A. B., "Large deflection analysis of uniformly loaded annular membranes," AIAA J. 1, 2111–2115 (1963).

[3] Way, S., "Bending of circular plates with large deflections," Trans. Am. Soc. Mech. Engrs. 56, 627–636 (1934).

[4] Keller, H. B. and Reiss, E. L., "Non-linear bending of circular plates," Comm. Pure Appl. Math. IX, 633–659 (1956).

[5] Hencky, H., "Uber den Spannungzustand in Kreisrunden Platten mit verschwindender Biegungssteifigkeit," Z. Math. Phys. 63, 311–317 (1915).

[6] Pifko, A. B. and Goldberg, M. A., "Comments on an iteration procedure for the large deflection analysis of initially flat membranes," Grumman Research Dept., Publication RM-232 (June 1964).

Surface Effects in a Pulsed Plasma Accelerator

William J. Guman* and William Truglio†

Republic Aviation Corporation, Farmingdale, N. Y.

Introduction

EXPERIMENTAL studies of several pulsed plasma accelerators on a thrust stand showed that a significant dropoff in impulse as well as changes in the plasma front velocity and plasma sheet structure could occur during a test that involves many thousands of consecutive discharges. The dropoff in impulse has been observed for varying electrode materials, insulator materials, energy per discharge levels, propellants, vacuum chambers and background pressures, polarity of the electrode assembly, initial surface preparation, and with pinch-type plasma accelerators as well as coaxial configurations (see Fig. 1).

The mechanisms responsible for observed changes that occur during continuous operation of the accelerator have been found to be related to the following surface effects: 1) outgassing of absorbed and adsorbed gas; 2) mass removal from the electrodes and insulator assembly due to the various erosion effects as well as the contribution of mass from loose particles, organic monolayers, and foreign matter such as trapped moisture, dust, etc.; 3) resistive changes due to thermal, chemical, and metallurgical changes at the electrode surface and deposition of ablated insulator material; and 4) viscous boundary-layer and current boundary-layer effects.

This note will present and discuss the techniques and some of the results of the experimental studies that have been carried out for evaluating items 1 and 2.

Studies Pertaining to Outgassing

Experiments carried out with the same initial electrode and insulator surface condition indicated that the magnitude of the impulse of the first few discharges of a test series could be changed appreciably by methods that affect the level of outgassing prior to data taking. For example, it was found that the impulse measured after a device had been operated several hundred consecutive discharges could be raised roughly 10 to 40% by venting the vacuum chamber to atmospheric pressure for periods less than 1 hr. Similarly, it was found that heating the accelerator in the vacuum environment to a temperature of about 640°R prior to operation would lower the initial impulse by roughly 18%. Pressurizing the interelectrode spacing at 70 psi for a period of 16 hr prior to evacuation and operation raises the initial impulse levels by roughly 10%.

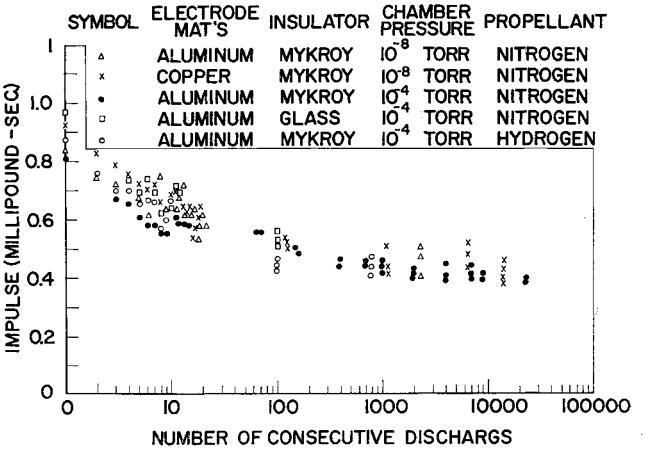

Fig. 1 Some representative impulse data.

A device was installed on the thrust stand which permitted data to be obtained on the quantity of gas driven off by outgassing during pump-down and during operation of the accelerator and which also permitted the electrode-insulator assembly to be isolated from oil vapor contamination during the pump-down cycle. This device was a remotely controlled capping mechanism that sealed off the interelectrode spacing from the vacuum chamber. Figure 2 shows the accelerator on a thrust stand with the capping mechanism in the withdrawn position, thus permitting accelerator operation. Figure 3 shows the capping mechanism sealing the interelectrode assembly from the vacuum chamber. This technique permitted evaluation of only that gas which is evolved from the surfaces in contact with the electrical discharge. Unlike weighing procedures, the accelerator is not handled, and the measurement could be carried out in the vacuum environment at any particular moment of interest.

To determine the quantity of gas desorbed during pump-down, the interelectrode spacing is sealed by the remotely controlled cap immediately after the normal evacuation

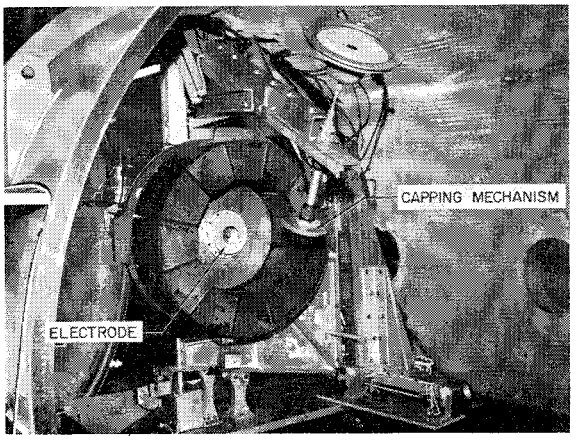

Fig. 2 Capping mechanism withdrawn.

Received March 23, 1964.

* Staff Engineer, Power Conversion Division. Member AIAA.

† Principal Research Engineer, Power Conversion Division.